Using Nonlinear-Elastic Stiffness at Small Displacement to Identify Damage in a Full-Scale Reinforced Concrete Building

Fabián Consuegra, Ph.D.[1]; Damon R. Fick, Ph.D., P.E., M.ASCE[2]; and Ayhan Irfanoglu, Ph.D., A.M.ASCE[3]

Abstract: In this paper, sensitivity of small-amplitude stiffness of a full-scale, three-story reinforced concrete flat-plate structure is investigated to assess development of damage during cyclic lateral load with up to 3.0% lateral drift ratio. The small-amplitude displacement tests were made at a maximum 0.03% drift ratio between the cycles of lateral loads causing mean roof drifts of 1.5% and 3.0% drift ratios. Results of the small-amplitude experimental program suggest that the building behaves as a nonlinear-elastic system at small displacement (i.e., drift ratio below 0.03%), and the small-amplitude stiffness compared at identical displacements can indicate damage from previous large-displacement cycles. It is shown that there is a robust and consistent relationship between stiffness and varying natural frequency measured at small displacements. As demonstrated, small-amplitude vibration properties may be an effective indicator of damage as long as a nonlinear-elastic model is used instead of a traditional linear model. **DOI: 10.1061/JPCFEV.CFENG-4506.**

Introduction

Small-amplitude displacement experimental data from the full-scale, three-story building shown in Fig. 1 were used to develop linear-elastic and nonlinear-elastic models to observe the sensitivity of small-displacement stiffness to the increasing damage observed from four cycles of lateral load testing of the full-scale structure to 0.2%, 0.5%, 1.5%, and 3.0% mean roof drift ratios. This range of deformation will be referred to as large-displacement drift and it has been extensively studied in the literature for this type of structure, in order to associate structural damage to large displacement (Elgabry and Ghali 1987; Farhey et al. 1993; Pan and Moehle 1992; Sozen and Siess 1963; Hwang and Moehle 2000; Durrani et al. 1995; Luo and Durrani 1995; Robertson et al. 2002; Hawkins et al. 1974). Given that monitoring large displacement in structures is seldom available, easy-to-record small-amplitude stiffness being related to large displacement is used to detect damage in the building specimen. Stiffness was statically measured between large load cycles at a maximum deformation of 0.03% drift ratio (0.254 mm top displacement), where no additional damage was induced, and accordingly elastic behavior was expected (Takeda et al. 1970). Small-amplitude dynamic measurements in the form of free and forced vibrations were performed at (1) the pristine condition prior to any cyclic lateral loading, (2) after the 1.5%-drift ratio cycle, and (3) after the 3.0%-drift ratio cycle where punching shear failure occurred in one of the slab-column connections. A nonlinear-elastic softening model led to an understanding of the building behavior measured in small displacements, better than that of the traditional linear model. Using the nonlinear-elastic model, it was possible to identify small-amplitude stiffness variations associated with damage in the building observed after the 1.5% and 3.0% drift ratio lateral load cycles by means of small-amplitude vibrations. Similar damage assessment could not be investigated for cycles 1 and 2 in Fig. 3, because those quasi-static tests were executed continuously and no dynamic test data were collected between the 0.2% and 0.5% drift ratio cycles.

The proposed damage identification approach by means of changes in natural frequencies of the structure is consistent with the widely known approach used by many researchers in the literature (Doebling 1996; Doebling et al. 1998; Chang et al. 2003; Salawu 1997; Sohn et al. 2003). Thus, in this investigation, variation in natural frequency is observed directly from the load-displacement curve as frequency depends on stiffness. However, rather than using a linear-elastic model, as done by many researchers (Neild 2001), this investigation expands on the results of previous researchers by using a nonlinear-elastic model at displacements below 0.03% drift ratio to identify damage from larger-scale displacement histories. The sensitivity of small-amplitude natural frequency and damping to displacement in reinforced concrete structures has been reported by Consuegra and Irfanoglu (2012). In the current paper, the focus is on the direct relationship between damage and stiffness measured at small displacements (i.e., no more than 0.03% drift ratio).

The novelty of the current research is to measure stiffness directly from the load-displacement curve that matches the nonlinear behavior identified from frequency measurements, both at small displacement. Nowadays, structural engineering for reinforced concrete structures continues to have nonlinear modeling strongly focused on large drift ratio studies (Tura et al. 2023; Fischinger et al. 2019; Ibarra et al. 2005; Kolozvari et al. 2019). Although there exist approaches based on nonlinear behavior at small-amplitude nonlinear response to detect damage in the fields of aerospace, mechanical, and civil, these may be cumbersome

[1]Head for Structural Division, Ingetec Ingenieros Consultores, Cra. 6 No. 30A-30, Bogotá, DC, Colombia (corresponding author). ORCID: https://orcid.org/0000-0002-7047-7002. Email: fabianconsuegra@ingetec.com.co

[2]Senior Research Engineer, Montana State Univ., Western Transportation Institute, P.O. Box 174250, Bozeman, MT 59717-4250. ORCID: https://orcid.org/0000-0002-1219-1495. Email: damon.fick@montana.edu

[3]Professor and Associate Head, Lyles School of Civil Engineering, Purdue Univ., West Lafayette, IN 47907. Email: ayhan@purdue.edu

Note. This manuscript was submitted on February 22, 2023; approved on January 5, 2024; published online on March 26, 2024. Discussion period open until August 26, 2024; separate discussions must be submitted for individual papers. This paper is part of the ***Journal of Performance of Constructed Facilities***, © ASCE, ISSN 0887-3828.

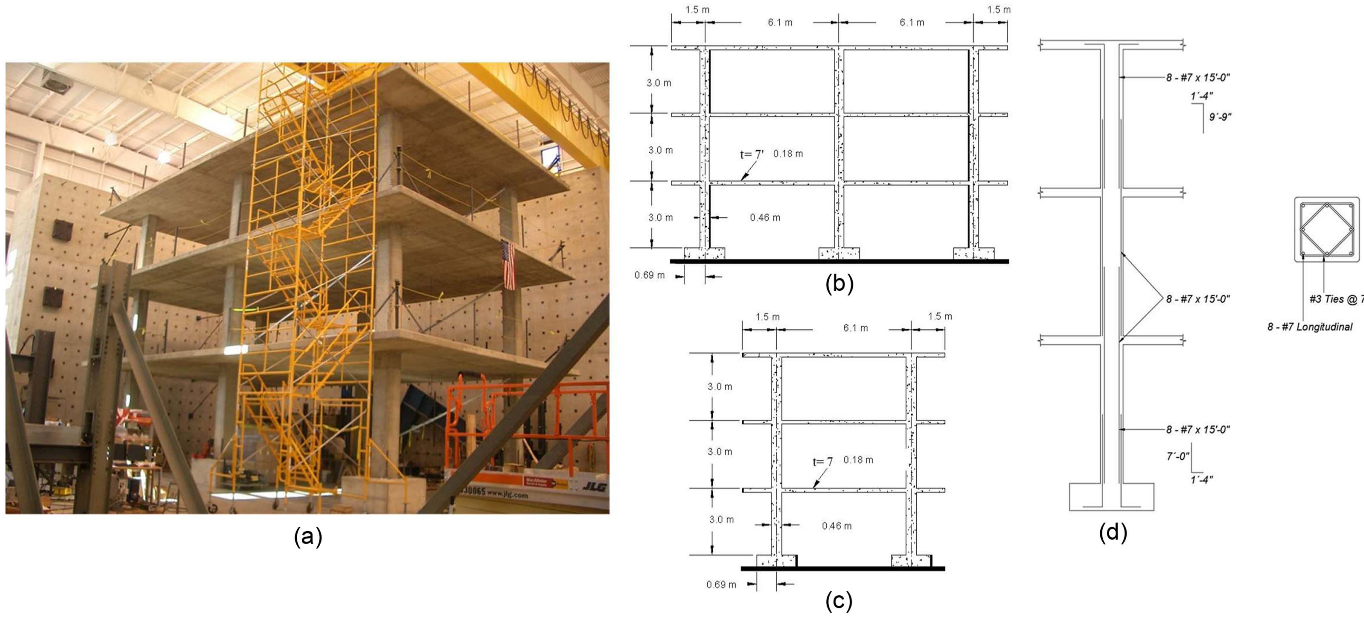

Fig. 1. Three-story RC flat-plate building.

(Farrar et al. 2007). Most of the nonlinear applications at small displacements in structural engineering have been found for fatigue in metals and very little has been done even for a single reinforced concrete beam (Neild 2001). This research provides a valuable example of small-amplitude nonlinear behavior being sensitive to damage in simple terms of stiffness observations in a full-scale building.

Comparison between Linear-Elastic and Nonlinear-Elastic Systems

The magnitude of a transfer function (TF) defined as the ratio between the response (displacement) and the input (force) for a linear-elastic SDOF system can be defined as shown in Eq. (1) (Chopra 1995)

$$|TF(\Omega)| = \frac{1/k}{\sqrt{[1-(\Omega/\omega)^2]^2 + [2\cdot\zeta\cdot\Omega/\omega]^2}} \tag{1}$$

where k, Ω, ω, and ζ = stiffness, excitation frequency, natural frequency, and equivalent viscous damping ratio, respectively. An experimental version of the TF is obtained through a series of harmonic forcing vibration tests where input force and displacement response are measured during steady-state condition. If the system is nonlinear so the stiffness becomes a function of displacement for instance, the TF in Eq. (1) becomes a function of displacement amplitude.

In order to illustrate the nonlinear effect in the calculation of a TF according to Eq. (1), consider a system where the secant stiffness k is a function of the displacement amplitude Δ, thus, $k = k_o\Delta^{-\alpha}$. The system was selected with a slight nonlinear behavior defined through a value of $\alpha = 0.015$ as shown in Fig. 2(a) and with the value of k_o selected equal to the stiffness in the pristine condition of the building specimen (Fig. 1). The exponential function selected for displacement dependence of stiffness is in accordance with experiments in the pristine condition of the building of this article [circle series and solid line in Fig. 5(a) are experimental results similar to Fig. 2(c)], as will be shown later. The selection of $\alpha = 0.015$ is also based on response measurements under pseudo-static loading of the building in the pristine condition. Fig. 2(d) shows the load-displacement curve before releasing the building to obtain free vibration records reported in Table 2. Two stiffness measurements, k_1 and k_2, are used to obtain the value for α, which allows for simulating the nonlinear behavior of the building in its pristine condition through the expression $k = k_o\Delta^{-\alpha}$. In Fig. 2(d), a dashed line that connects origin to final test datum at 0.52 mm displacement is used to enhance visualization of the nonlinear softening behavior. A comparison of the corresponding load-displacement relationship with that of a linear system ($\alpha = 0$) can be seen in Fig. 2(b), where almost no difference can be seen between the curves (both from numerical simulation). Fig. 2(c) shows the calculated TF for the nonlinear system through Runge-Kutta (Oppenheim et al. 1999) by numerically solving the equation of motion stated for a nonlinear-elastic system (The MathWorks 2004). Also, in Fig. 2(c), the best fit calculated through a square root of the sum of squares (SRSS)-error method according to the theoretical linear TF of Eq. (1) is plotted (parameters for the linear solution were selected such that the full SRSS representing the difference between nonlinear and the linear transfer functions was minimized). It can be seen that given the slight level of nonlinearity ($\alpha = 0.015$), natural frequencies of the two systems identified by the resonance peak of the curve (maximum), are similar. However, values of the linear TF to the left of the peak are larger than those from the nonlinear system TF (for frequencies below 1.86 Hz), and the opposite situation is observed to the right side of the peak. An error estimate of the linear fit according to Eq. (1), obtained as the point-to-point difference with respect to the actual (nonlinear) TF through an SRSS calculation, is about 30%. Also, the stiffness estimate from the linear model differs by 10% from actual stiffness of the nonlinear system at initial displacements represented by a plateau in Fig. 2(a).

A theoretical frame of reference for the behavior of nonlinear-elastic systems like the one used for the present study is cited in the literature as the Duffing oscillator (Kovacic and Brennan 2011) and the nonlinear-stiffness representation has been used in different engineering applications (Adams 2010; Feldman 2006). This type of nonlinearity makes the so-called nonlinear softening system due to the fact that stiffness decreases as displacement (distortion) is

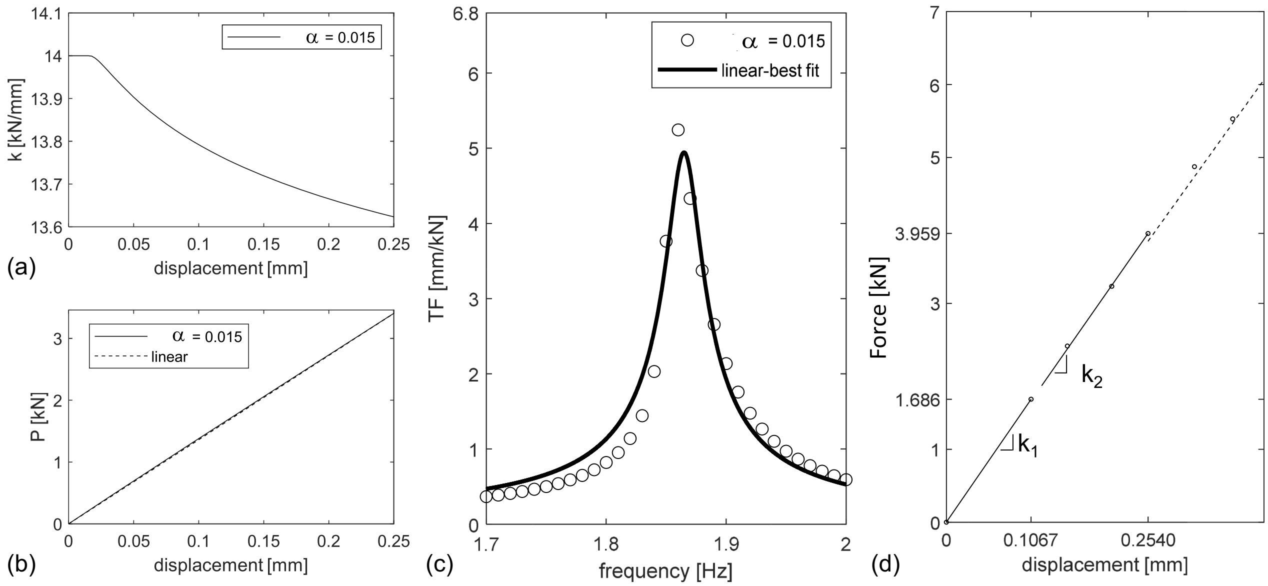

Fig. 2. Simulated response of a nonlinear system and comparison with a linear system: (a) stiffness-displacement relationship; (b) load-displacement curve; (c) TF of actual nonlinear system and its linear model fit; and (d) pseudo-static loading before obtaining free-vibrations records in building of Fig. 1.

increased, and as will be shown later, it is suitable for the description of small-amplitude behavior of the reinforced concrete building used in this paper. Even though nonlinearity has been broadly used for structural modeling of reinforced concrete structures for large displacements associated with reinforcement yielding (Clough and Penzien 1975; Eberhard and Sozen 1989; Moehle and Sozen 1978; Iwan and Gates 1979; Lakshmanan et al. 1991), the mentioned stiffness nonlinearity (elastic) in this article is observed at small displacements (below 0.03% drift ratio).

A similar comparison between linear and nonlinear systems shown in Fig. 2 can be seen in Fig. 5 for the experimental results of the 3-story reinforced concrete flat-plate building shown in Fig. 1. Two different types of forced-vibration results, and therefore, two corresponding experimental TFs, are shown in Fig. 5 (circles and squares). The first TF identified as *non-constant-displacement response* (circle series) corresponds to the traditional experiment where the dynamic actuator is set to a constant-displacement amplitude (stroke) value Δ_{actuator}, so each frequency run produces a different force in the building via the expression $F = m\Omega^2\Delta_{\text{actuator}}$, and the building displacement is simply different for each excitation frequency Ω. The second type of experimental TF in Fig. 5, identified as *constant-displacement response* (square series), was obtained such that the actuator amplitude Δ_{actuator} is modified at each excitation frequency Ω in order to produce the same target displacement in the building. Therefore, this type of TF corresponds to a set of experiments with an identical peak displacement response at each frequency Ω, so the building has the same secant stiffness in each test, as if it were a linear system. As stated previously, values of stiffness k_o and nonlinearity factor α for the simulated SDOF system in Fig. 2 were selected to represent the pristine condition of Fig. 5. Based on the experimental protocol for the two types of TFs, note that comparison in Fig. 5(a) between the circle series [linear, Eq. (1) used with constant k assumed] and the square series (nonlinear TF) in the pristine condition, depicts a similar comparison of that of simulated responses in Fig. 2(c). It can be observed in Fig. 5(a) that even in pristine condition, the building exhibits noticeable levels of nonlinear-elastic behavior at small displacement. A more detailed discussion regarding the TF measured in the building specimen will be further presented in the "Experimental Program" and "Comparison" sections next below.

Experimental Program

Cyclic Quasi-Static Tests

The test specimen (Fig. 1) was a full-scale, two-span by one-span, three-story reinforced concrete flat-plate structure of six columns spaced at 20 ft (6.1 m) in each direction and supporting a 7 in. (~20 cm) thick slab at each story. Fig. 1(a) is a photograph of the constructed full-scale specimen, and Figs. 1(b and c) show the east and north elevations views, respectively. Fig. 1(d) shows the column reinforcement detail, consisting of 8 #7 bars (7/8 in or #22 bar in metric size) or 1.5% longitudinal reinforcement ratio. Slab was provided with reinforcement amounts of 0.27% (bottom) and 0.53% (top) for both directions. Each footing was secured to the 33 in. (83.8 cm)-thick laboratory strong floor with four 1–3/8 in. (34.9 mm) Dywidag Threadbars, each post-tensioned to 100 kip (444.8 kN). A superimposed load of 13.3 psf (0.64 kN/m^2) was added at each floor by means forty 55-gallon barrels (0.208 m^3) filled with water.

The structure was quasi-statically loaded by applying lateral forces at each floor in the longer north-south direction of the structure. The applied loads followed a triangular distribution over the height of the specimen and followed a 3:2:1 ratio at the roof, second floor, and first floor slab levels (Fick 2010). Fig. 3 summarizes the four quasi-static loading cycles with roof drift ratios of 0.2%, 0.4%, 1.5%, and 3% in the form of roof drift ratio versus base shear ratio coefficient, i.e., ratio of the base shear force as a percentage of total weight, respectively. The structure suffered punching shear failure at roof drift ratio of 3.0%, as shown in Figs. 4(a and b), consistent with the traditional failure mode in this type of structure (Megally and Ghali 2000; Ghali et al. 1976; Pan and Moehle 1989; Morrison et al. 1983). Dynamic tests were performed at three stages of the quasi-static cyclic testing as indicated in Table 1: (1) before cycle 1

J. Perform. Constr. Facil., 2024, 38(3): 04024011

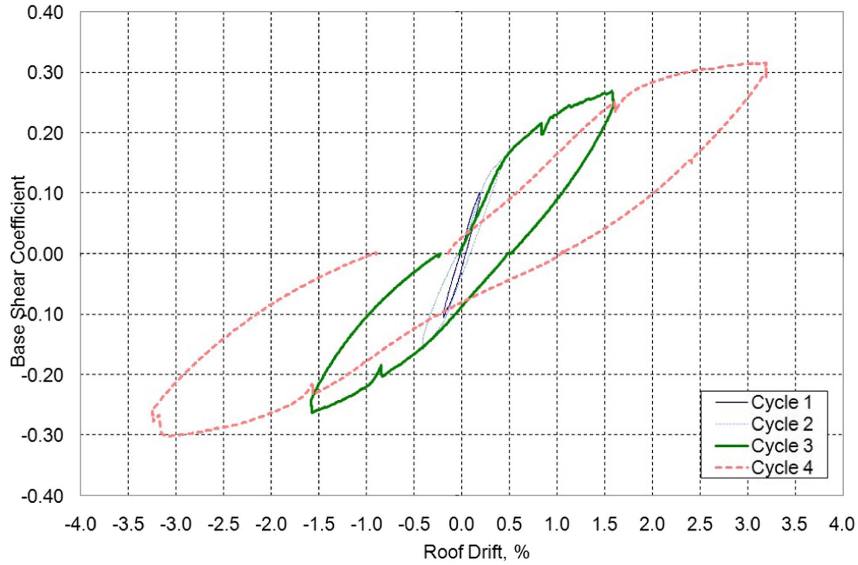

Fig. 3. Load-displacement response of a three-story flat-plate structure. (Data from Fick 2010.)

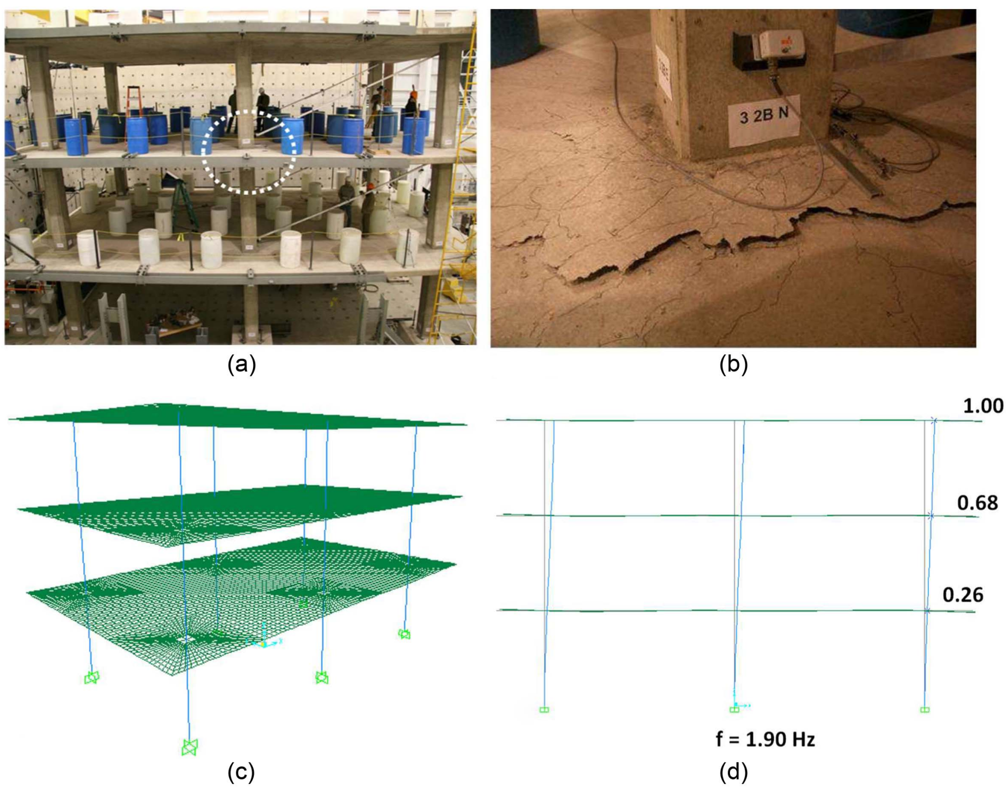

Fig. 4. Punching shear failure location and finite element model.

(i.e., as-built pristine condition), (2) after cycle 3 (i.e., after 1.5% roof drift ratio), and (3) after cycle 4 (i.e., after 3% roof drift ratio).

Small-Amplitude Dynamic Tests

Table 1 summarizes the small-amplitude vibration tests performed in the building at displacement levels below 0.03% overall drift ratio, at different stages of the quasi-static cyclic testing that produced structural damage in the building. The dynamic tests consisted of ambient, free, and forced-vibration tests, performed before and after some of the quasi-static cyclic tests applied to the building (up to 3 % drift ratio). 5g-full-range output accelerometers were used in conjunction with a 19-bit acquisition system which can detect displacements as small as one-thousandth of a millimeter if recorded at steady-state frequency of 2 Hz (when noise is ignored in the estimate).

Forced-Vibration Tests

Forced-vibration tests were done by use of a linear actuator placed on the roof-level of the building and connected to a cart with

Table 1. Experimental program in the RC building

Test	Description
Dynamic	
Free vibration	Set of pull-release tests on each slab-level NS direction. $\Delta_{max} = 0.508$ mm roof.
	Set of pull-release tests on roof-level EW direction. $\Delta_{max} = 0.508$ mm roof.
Forced-vibration	NS dir. roof-level excitation by use of actuator. $\Delta_{max} = 0.254$ mm roof
Ambient vibration	1-h record of ambient vibrations
Quasi-static (cycles 1, 2 and 3)	Series of pseudo-static loading cycle. $\Delta_{max} = 13.7$ cm roof (1.5% overall drift ratio)
Dynamic	
Free vibration	Set of pull-release tests on each slab-level NS direction. $\Delta_{max} = 6.35$ mm roof.
	Set of pull-release tests on roof-level EW direction. $\Delta_{max} = 1.016$ mm roof.
Forced-vibration	NS dir. roof-level excitation by use of actuator. $\Delta_{max} = 2.54$ mm roof
Ambient vibration	1-h record of ambient vibrations
Quasi-static (cycle 4)	Series of pseudo-static loading cycle. $\Delta_{max} = 27.4$ cm roof (3.0% overall drift ratio)
Dynamic	
Free vibration	Set of pull-release tests on each slab-level NS direction. $\Delta_{max} = 1.27$ cm roof.
	Set of pull-release tests on roof-level EW direction. $\Delta_{max} = 2.03$ mm roof.
Forced-vibration	NS dir. roof-level excitation by use of actuator. $\Delta_{max} = 2.54$ mm roof
	EW dir. roof-level excitation by use of actuator. $\Delta_{max} = 1.778$ mm roof
Ambient vibration	1-h record of ambient vibrations

weight. Harmonic dynamic force was transmitted to the building as the linear actuator reacted against the roof slab-level. An accelerometer placed on top of the cart allowed estimation of the dynamic force. The dynamic force computed using the cart accelerations allowed verification of load measured by the load cell of the actuator. Harmonic excitations with forcing frequencies [Ω in Eq. (1)] in the vicinity of the natural frequency of interest were used. Force-input and acceleration-output of the building were recorded for 200 seconds after steady-state response was observed, with 1,000 mV/g-sensitivity accelerometers in environment-controlled conditions in the laboratory to record data with precision such that the ratio between the minimum displacement amplitude of interest and the system precision was about 1,000.

Fig. 5 shows TFs estimated from three different stages of damage of the building that are associated to the large displacement of quasi-static cycles, as described in Table 1. Fig. 5(a) shows TFs in the as-built condition with zero past displacement, Fig. 5(b) shows TFs after the building was subjected to 1.5% overall drift ratio, and Fig. 5(c) shows TFs after the building was subjected to 3.0% overall drift ratio. In each damage condition, three types of TFs were obtained and are described next. The nonconstant-displacement response TF (circle series) comes from the standard type of harmonically forced-vibration tests, where each excitation frequency (Ω) is set with a constant stroke in the actuator so the force applied to the building is different in each frequency step. This results in different peak roof lateral displacement amplitudes in the building when excited at different forcing frequencies. The constant-displacement response type of TF (square series) was performed in a manner such that at each frequency the actuator stroke was selected to result in the same peak roof-lateral displacement of 0.254 mm. In these latter tests, the structure responds at an identical peak displacement level so any nonlinear-stiffness behavior would apply equally at each forcing frequency, as the dynamic response of the structure is displacement-controlled (i.e., identical peak displacement) and

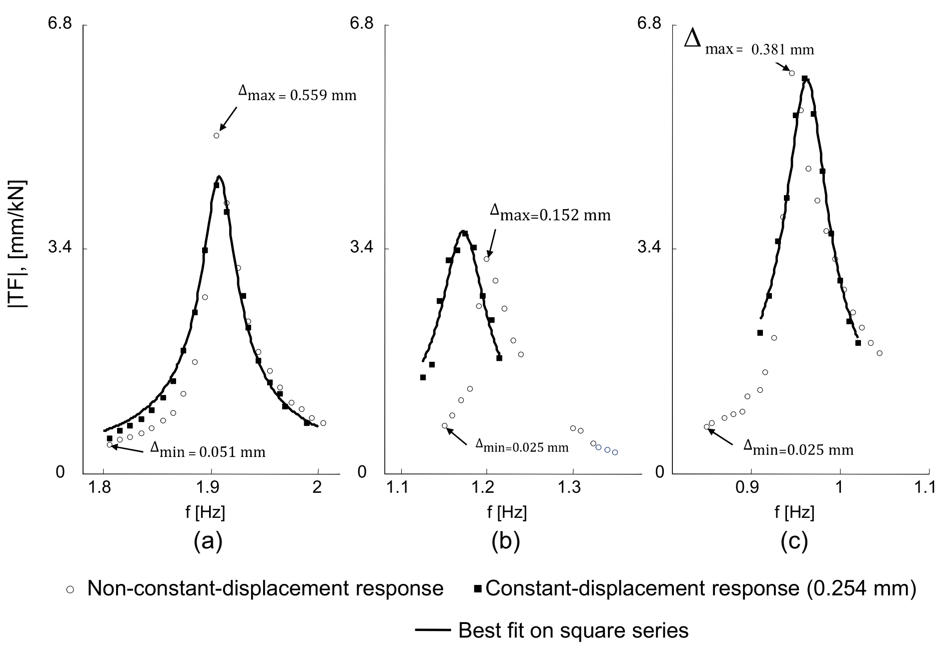

Fig. 5. Transfer function of the building in different structural conditions: (a) pristine; (b) after 1.5% drift ratio; and (c) after 3.0% drift ratio.

the structure exhibits identical secant stiffness at each forcing case. The third type of TF plotted is the linear best fit achieved with Eq. (1) on the experimental data from the constant-displacement response TF (square series) by selecting the parameters of natural frequency ω, total top-stiffness K, and damping ratio ζ. For a linear system, the two types of experimental TFs, i.e., for nonconstant-displacement response and for constant-displacement response types, would be identical relative to different displacement amplitudes as a normalization process is implicit in true linear-elastic structures. However, given the nonlinear-stiffness nature of the building, there are differences in the two types of experimental TFs (circle and square series) obtained from actual buildings such as the structure studied herein. The protocol for obtaining the two TFs presented differs from protocols executed in other forced-vibration tests performed in similar structures (Yu 2005). A comparison of the two experimental TFs in Fig. 5 shows that even at small displacement levels and regardless of the damage condition, the building exhibited nonlinear-elastic behavior in a similar manner to that simulated in Fig. 2. Similar to the best-fit curve shown in Fig. 5, a fitting procedure (not shown in Fig. 5 for clarity purposes) was performed on the nonconstant-displacement TF data, thus, on the circle series of data. In order to verify the adequacy of Eq. (1) in estimating the response of a nonlinear system, error estimates for the case of nonconstant-displacement and constant-displacement TFs were compared. The error in each case was defined as the SRSS of the differences between experimental and best-fit analytical TF estimates. The ratio of error estimates between nonconstant-displacement TF (nonlinear behavior) and constant-displacement TF (enforced linear-elastic behavior), obtained for the pristine condition of the building, was 20.8, which shows the remarkable relative inaccuracy of a linear-elastic model [Eq. (1)] to predict the natural behavior of the nonlinear-elastic system, whereby the error of a linear model to predict the actual (nonlinear) building behavior is more than 20 times the error of the same model to predict behavior of the same building enforced to behave linearly. Error estimates of the linear model to predict the experimental nonconstant-displacement TF and the constant-displacement TF were also obtained for the building conditions after 1.5% and 3.0% drift ratios. Similar to the error ratio obtained for the pristine condition (ratio of more than 20), the ratio of error estimates for the conditions of the building after 1.5% and 3.0% drift ratio, respectively, were 4.8 and 16.1. These two error ratios confirm the inaccuracy of the linear-elastic model even at small displacement, due to the fact that the building exhibited nonlinear behavior regardless of the damage levels imposed by large displacements. Based on the best fit of Eq. (1) on the constant-displacement response data (square series), the estimates of natural frequencies of the building associated with results plotted in Fig. 5 are 1.91 Hz, 1.17 Hz, and 0.96 Hz for the three structural conditions; thus, different natural frequencies were obtained for the same small displacement (0.254 mm roof drift) at different damage levels. Variations of observed natural frequencies of reinforced concrete structure have been reported in the literature at small displacements with no apparent damage (Clinton et al. 2006; Celebi 1996). However, the current study shows that regardless of the damage conditions in the building, a nonlinear-elastic model is more suitable for damage identification by means of changes in small-amplitude stiffness.

Free Vibration Tests

Free vibration tests in the building were performed through a quick-release mechanism installed at the roof-level. The structure was given an initial target displacement and released from rest so that it vibrates freely with zero initial velocity. A sensor data sampling rate of 2,000 samples/s was used in all tests with similar sensor configurations to that used in forced-vibration tests. A summary of natural frequencies estimated through a Fast Fourier Transform (FFT) (Bendat and Piersol 1986) of the free vibration response obtained for each of the structural conditions of the building is shown in Table 2. Each test is identified by its initial displacement Δ_{roof} selected as one of the nominal values of 0.5, 1.0, or 2.5 mm. The natural frequency of the building reported in Table 2 was identified by the largest peak in the Fourier spectrum of the corresponding vibration record. The maximum coefficient of variance for the natural frequency measured in tests with similar displacement and reported in Table 2 was 0.8% (for instance tests 2-1, 2-2, and 2-3), which indicates the elastic behavior of the building (repeatability of tests), and also shows the consistent relationship between natural frequency and displacement amplitude (nonlinear-stiffness behavior). Therefore, it can be seen in Table 2 that for a given structural condition, the frequency decreases as the initial displacement is increased. This variation in frequency resembles the nonlinear softening behavior of the building represented by the α exponent in Fig. 2.

Table 2. Free vibration response summary

Test	Δ_{roof} (mm)	P (kN)	f_1 (Hz)
	As-built		
1-1	0.511	7.9	1.92
1-2	0.521	8.1	1.92
1-3	0.508	7.9	1.91
	After 1.5% drift ratio		
2-1	0.516	3.5	1.26
2-2	0.516	3.6	1.26
2-3	0.521	3.7	1.27
2-4	1.024	6.9	1.24
2-5	1.026	6.8	1.23
2-6	1.026	6.8	1.23
2-7	2.545	14.5	1.17
2-8	2.553	14.1	1.16
2-9	2.555	14.0	1.15
	After 3.0% drift ratio		
3-1	0.406	2.0	0.99
3-2	0.511	2.0	1.00
3-3	0.513	2.0	0.99
3-4	1.029	3.9	0.96
3-5	1.049	4.0	0.96
3-6	1.077	3.9	0.96
3-7	2.565	8.8	0.93
3-8	2.578	8.8	0.93
3-9	2.565	8.7	0.93

Fig. 6 shows some examples of the Fourier spectra where the natural frequencies identified as the largest peak were reported in Table 3, scaled to the number of sample points to make them comparable (Flandrin and Stöckler 1999). In Fig. 6(a), the natural frequency from 0.5-mm tests at different structural conditions of the building decreases as past-large displacement is increased. Thus, damage in the building causes reduction of small-amplitude vibration frequency when a comparison is made at identical displacement (0.5 mm). In other words, the small-amplitude natural frequency is sensitive to past-large displacement in the building, even though small and large displacement differ by a factor of more than 300: for instance, test 3-1 in Table 2 performed at 0.004% drift ratio (the drift is obtained as 0.406 mm/9 m) was sensitive to previous 1.5% drift ratio tests. Fig. 6(b) shows that for the condition after the building experienced 3.0% drift ratio, the behavior of the building at small displacement may be also represented as that of a nonlinear softening system. Fig. 6(b) shows how the largest peak of

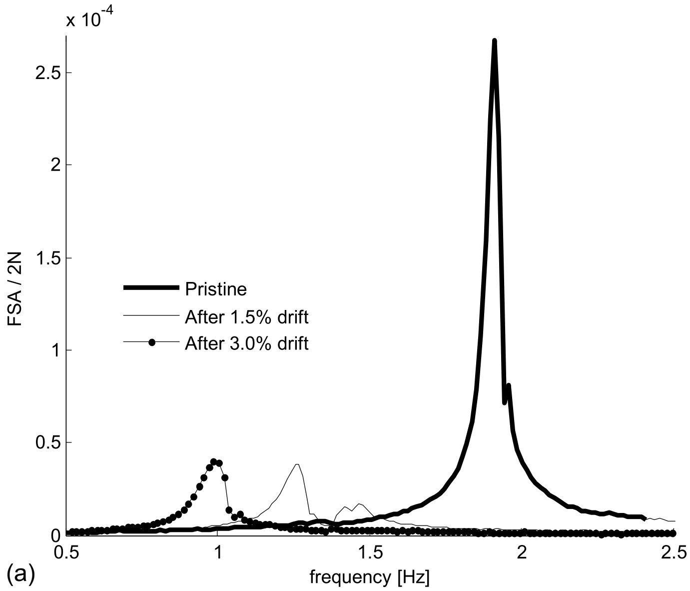

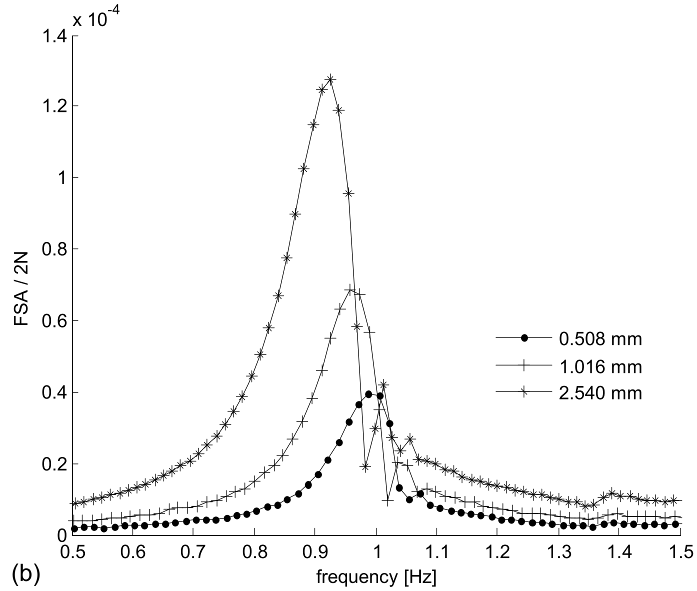

Fig. 6. Natural (peak) frequency from Fourier spectrum amplitude: (a) natural frequencies for the same small displacement of 0.508 mm at different past-large displacement stages; and (b) natural frequency for the after-3.0% peak drift ratio stage at different small displacements.

Table 3. Stiffness values from static and dynamic tests (kN/mm)

		Small displacement for testing											
		0.254 mm			0.508 mm			1.016 mm			2.54 mm		
Row	Test/condition	STA	DYN	r	STA	DYN	r	STA	DYN	r	STA	DYN	R
1	At pristine	—	14.0[a]	1.06	—	—	—	—	—	—	—	—	—
2	0.2% drift ratio cycle	13.2[a]	—	—	13.3	—	—	13.4	—	—	13.3	—	—
3	1.5% drift ratio cycle	8.1	—	—	7.5	—	—	6.9	—	—	6.2	—	—
4	After 1.5% drift ratio cycle	—	6.6[b]	1.06	—	6.3[c]	1.12	—	5.7[d]	1.09	—	5.4[e]	1.21
5	3.0% drift ratio cycle	6.2[b]	—	—	5.6[c]	—	—	5.2[d]	—	—	4.5[e]	—	—
6	After 3.0% drift ratio cycle	—	3.7	—	—	3.2	—	—	3.2	—	—	3.0	—

Note: STA: static stiffness, DYN: dynamic stiffness; r: stiffness ratio = DYN/STA; superscripted letters a through e indicate pair of values from specific dynamic and static tests that can be compared.

the spectrum shifts to the left as the initial displacement in the test is increased. This numerical variation of natural frequency has been reported in Table 2. It is similar to the nonlinear softening behavior assumed for the system in Fig. 2 (nonlinearity represented by the α exponent).

Comparison of Stiffness from Static and Dynamic Tests

The quasi-static tests shown in Fig. 3 were performed through a linear load distribution of lateral forces F_1, F_2, and F_3, being applied at the first, seconds and third floors, respectively. Such a set of forces can be summarized through a column vector $\{F\}$ and the corresponding displacements at each floor defined as $\{u\}$. The vectors $\{F\}$ and $\{u\}$ were used to estimate stiffnesses of the building at displacement amplitudes similar to those from dynamic tests. The building was represented by means of a single lateral DOF at each floor, therefore the equilibrium equations represented by $\{F\} = [K]\{u\}$ were solved to calculate each of the three terms in the stiffness matrix $[K]$. This calculation was performed for each state of Fig. 3 represented by the sum of all forces plotted on the vertical axis and the roof displacement u_3 plotted on the horizontal axis. A total top-stiffness was calculated as the in-series sum of stiffnesses of the three stories, in order to simplify the stiffness comparison with the dynamic testing where external load was applied at the roof only. The precision of load (hydraulic actuator) and displacement (string potentiometer) measured during static tests were 20 lbf (0.089 kN) and 0.001 in. (0.025 mm); thus, displacement precision of static tests was equal to one-tenth of the smallest displacement considered (0.01 in. = 0.254 mm used in dynamic tests). Based on a linear estimate from Table 2, the top-floor load applied so as to produce the smallest displacement of dynamic tests equal to 0.254 mm is about 1 kN (2 kN produces a displacement of 0.406 mm in test 3-1), which is more than 10 times the force precision of static tests. Given the comparison between smallest force and displacement quantities of static tests and their corresponding precision levels, precision is about one-tenth of the smallest magnitude of interest. Accordingly, estimates of stiffness from static tests at small displacement are considered accurate enough in comparison with the high-precision measurements of dynamic tests described in the section "Small-Amplitude Dynamic Test." Fig. 7(a) shows the story shear versus the story drift for the static cycle of 3.0% drift ratio from Fig. 3. The story stiffnesses shown in Fig. 7(a), varying with displacement, are the secant slopes of the curves in Fig. 3. This stiffness variation is observed even at the

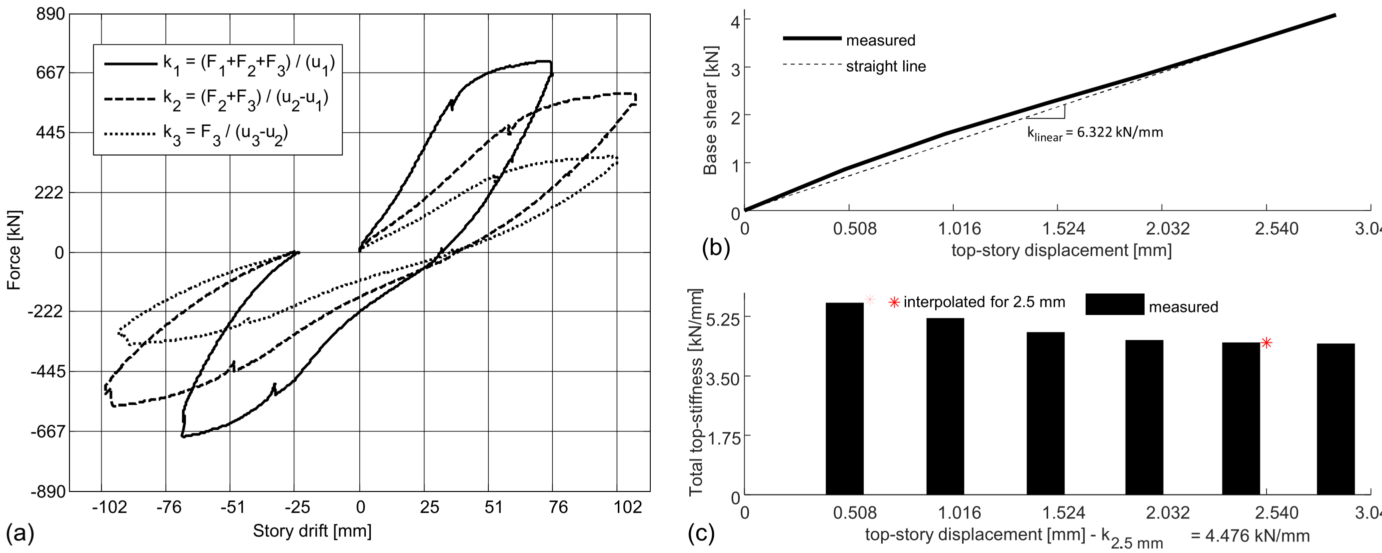

Fig. 7. Small-amplitude-displacement stiffness estimates from quasi-static test at 3.0%-drift ratio cycle.

beginning of the cycle where a linear-elastic assumption is commonly made. This nonlinearity represents the same nonlinearity presented in the section "Experimental Program" through vibration testing. The story drift used in Fig. 7(a) is not allowed to relate the nonlinearity to the top (roof) displacement, which is explicitly the limit set for the elastic behavior in the building. Fig. 7(b) shows the total base shear of Fig. 7(a) versus the top-story displacement, plotted up to a maximum displacement of 2.5 mm (0.03% drift ratio) that represents the elastic behavior in concrete sections (Takeda et al. 1970). It can be seen that at small displacement levels there is a clear nonlinear behavior of the building when compared with the straight-line reference that represents a constant stiffness. Fig. 7(c) shows variation of total top-stiffness calculated from actual measurements through the matrix solution presented in this Section, with an estimate of 4.476 kN/mm for a target displacement level of 2.5 mm (0.03% drift ratio). This estimate of stiffness is 30% smaller than the straight-line stiffness shown in Fig. 7(b) (6.322 kN/mm). This estimate is included in the full comparison of stiffness values in Table 3. Variation of stiffness values in Fig. 7(c) is about 27% and this variation may be more apparent when tracing a specific story stiffness, given the fact that total (equivalent) stiffness (a measure of overall roof drift stiffness) is less sensitive to any particular story-stiffness variation.

Fig. 8 shows each story stiffness as a function of the story drift for the static cycles of 1.5% and 3.0% drift ratio. The total top stiffness obtained as the in-series summation of stiffnesses is also shown in Fig. 8. Notice that the horizontal axis limit corresponds to the elastic limit of 0.03% drift ratio converted to the displacement of one single story (0.03% × 3 m–1 mm). The quasi-static cycle of 0.2% drift ratio has been left out of Fig. 8 based on a very small amount variation of stiffness exhibited in this condition, as will be shown in Table 3. Fig. 8 shows that the total top-stiffness of the

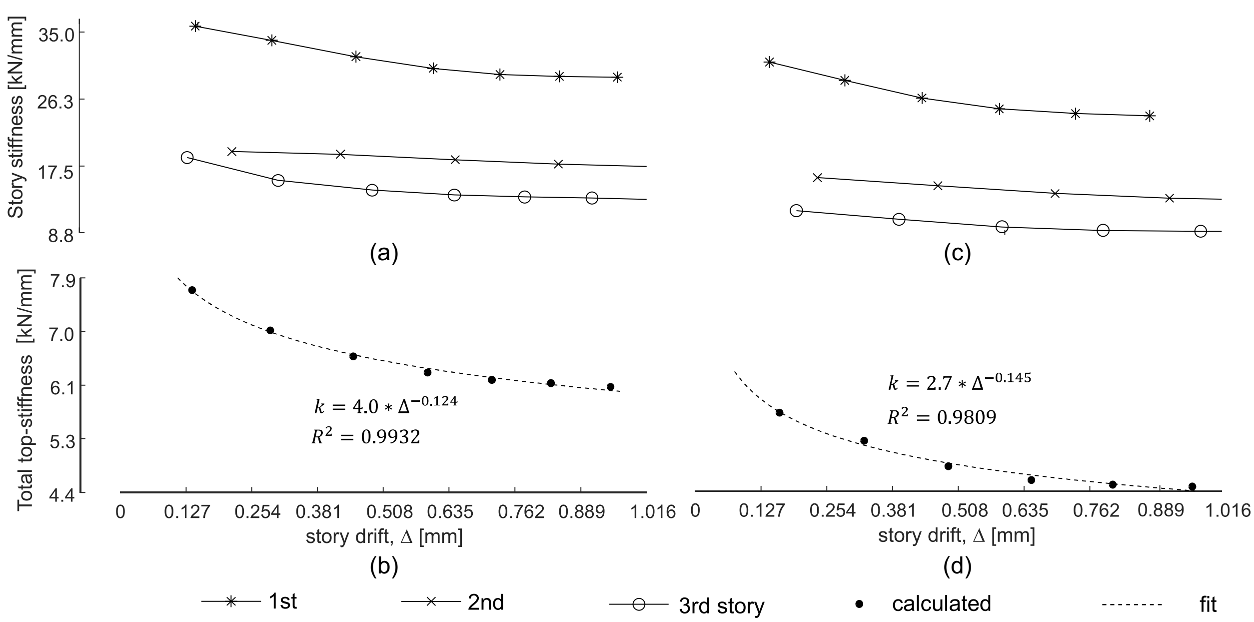

Fig. 8. Estimates of total top-stiffness for static tests: (a and b) individual and total stiffnesses for 1.5%-drift ratio cycle; and (c and d) Individual and total stiffnesses for 3.0%-drift ratio cycle.

J. Perform. Constr. Facil., 2024, 38(3): 04024011

building varies with displacement. Figs. 8(a and b) correspond to the 1.5% drift ratio cycle while Figs. 8(c and d) correspond to 3.0% drift ratio cycle. Figs. 8(a and c) show that first (ground) story is the story most sensitive to displacement. However, the contribution of ground story stiffness to the total equivalent stiffness is less compared to the stiffness of other stories based on their in-series contribution. Maximum variation of total top-stiffness for the data plotted is 30% and 40% for 1.5%- and 3.0%-drift ratio cycles, respectively. On both conditions (1.5% and 3.0% drift ratio cycles), a power function has been fitted to data whose fitting and correlating values indicate good agreement with experimental data. The exponent in the fitted functions resembles the α value used in the numerical simulation of Fig. 2, with values of $\alpha = 0.124$ and $\alpha = 0.145$ for the two conditions. These values correspond to higher degrees of nonlinearity than that of the numerical simulation in Fig. 2, which is in good agreement with the measured pristine condition in Fig. 5(a), where the maximum roof displacement was set to 0.559 mm. Given that maximum roof displacement in Fig. 8 is 2.54 mm, it is concluded that nonlinearity increases for larger values of small displacement [Fig. 8 corresponds to small displacement but larger than the displacement of pristine condition in Fig. 5(a)].

Table 3 shows the comparison of stiffnesses obtained from quasi-static ("STA") and dynamic ("DYN") tests at small displacements bounded by 2.54 mm, thus an overall drift ratio of 0.03% where elastic behavior has been assumed (Takeda et al. 1970). At such a level of drift, no additional damage is incurred.

In Table 3, dynamic results come from the forced-vibration results obtained through the constant-displacement response TF as described in the section "Forced-Vibration Test" and shown in Fig. 5. Results from static tests shown in Table 3 were obtained similarly to the procedure presented in Figs. 7 and 8. Column r corresponds to the stiffness ratio of dynamic to the static test. Stiffness values marked by superscripted letters a thru e in Table 3 (values in row 1 linked to values in row 2, and values in row 4 linked to values in row 5) indicate the pair of values from dynamic and static tests that can be compared to obtain factors r. This set of comparisons is limited based on the chronological order of tests performed (Table 1), such that comparisons are made without unfairly considering additional damage to the building. Comparisons made this way enforce that the sensitivity of stiffness is strictly evaluated due to large-past displacement. The only reasonable comparisons of stiffnesses for damage identification purposes were: (1) dynamic result in the pristine condition in row 1 to static result at beginning of 0.2% drift ratio cycle in row 2, and (2) dynamic tests after 1.5%-condition in row 4 to static tests at beginning of 3.0% drift ratio cycle in row 5. An average r-value of 1.1 indicates the consistency between measurements, so tracing the stiffness variation in the building at small displacement can be done by means of either static or dynamic testing. The nonlinear softening type of behavior of the building at small displacement observed in free and forced vibrations of the "Forced and Free-Vibration Test" sections is confirmed through static measurements from the section "Cyclic Quasi-Static Tests," as the stiffness decreases for increases in small displacement regardless of the damage condition. This can be seen by comparing stiffness values along a given row of Table 3. Such behavior is observed in all measurements from static tests, except for 0.2% drift ratio at row 2 where stiffness varies by about 1% due to the absence of damage introduced to the building up to that point. This insensitivity of the total top-stiffness is consistent with the fact that for early stages of testing (like that of pristine condition simulated in Fig. 2 and comparable to condition prior to 0.2% drift ratio cycle), a representative value of $\alpha = 0.015$ produces less than 4% variation between 0.254 mm and 2.54 mm of displacement, according to the analytical expression $k = k_o\Delta^{-\alpha}$. This small variation of stiffness may be experimentally undetectable in the pristine condition, and this may be the reason for the 0.2% drift ratio in row 4 of Table 3, which shows almost no variation for the total top-stiffness. Despite the insensitivity of stiffness to small displacement observed in the pristine condition, the sensitivity was clearly observed for the cycles with 1.5% and 3.0% peak drift ratios, i.e., once damage to the building has been imposed. Consistent with data from the damaged building, as will be explained next, stiffness variations through the analytical expression for the cycles of 1.5% and 3.0% drift ratio in Fig. 8 are 33% and 40%, respectively.

Static and dynamic tests do not produce identical estimates of stiffnesses (r is not 1.0), due to the fact that the load distribution patterns for the two tests enforce different deformed shapes in the building. While quasi-static tests correspond to linearly variation with floor elevation (inverted triangle), the forced-vibration tests contain inertial forces proportional to the natural mode shape. The deformed shape of the building measured at small displacement of quasi-static tests was {0.20, 0.72, 1,00} while the first mode shape of the building observed through modal identification was {0.26, 0.66, 1.00}. Modal identification on the experimental data was verified by comparing with results from a 3D finite element model built for the pristine condition (SAP2000), as shown in Fig. 4. The model consisted of 17,097 nodes, 18 frames, and 16,200 shell elements. ACI formulation was used to calculate the concrete modulus of elasticity used (ACI 2002). The fundamental mode natural frequency and mode shape of the FE model are within 3% difference of the experimental results shown for the pristine condition in Figs. 5 and 6, and Table 2. When comparing the two shapes in static and dynamic testing scenarios, it can be seen that while dynamic testing is engaging more contribution of the stiffest story (first) than that of the static test, making the system stiffer in general, the static test drift is concentrated in a more flexible story (second) which makes the building more flexible (story deformation of second story in static test is 0.52 versus 0.40 of dynamic test). The building responds stiffer during dynamic tests than during static. This is represented by r-values larger than 1.0 in Table 3.

In Table 3, it can be seen that small-displacement stiffness is always sensitive to damage caused by past-large displacement, as long as the comparison of stiffness is done at identical displacement levels, i.e., when stiffness values along a given column of the table are compared. Rather than the use of a single column to compare stiffnesses, if the comparison is erroneously done at different displacement amplitudes, the observation would lead to erroneous interpretation such that the stiffness is insensitive to damage or even worse, that stiffness could increase after damage. Consider, for instance, in Table 3, the comparison from dynamic tests before and after the 3.0% drift ratio cycle (rows 4 and 6), so the stiffness decrease can be correctly calculated through four pairs of values associated to displacement amplitudes of 0.254, 0.508, 1.016, and 2.54 mm. The four comparisons are: from 6.6 to 3.7, from 6.3 to 3.2, from 5.7 to 3.2, and from 5.4 to 3.0 kN/mm. The average ratio of stiffness decrease in those four comparisons is 55%. A reduction of 45% of stiffness was observed due to damage caused in the building by the 3.0% drift ratio cycle. The coefficient of variation of the four ratios is less than 5%, which indicates the consistency and equivalence in the damage identification if identical displacement amplitude is selected for the comparison. However, if stiffness measured at 2.54 mm before 3.0% drift ratio cycle (5.4 kN/mm, dynamic, row 4) is compared to stiffness measured at 0.254 mm during 3.0% drift ratio cycle (6.2 kN/mm, static, row 5), a fictitious increase of 15% in the stiffness would be concluded. An adjusted version of this comparison would lead to almost no variation of stiffness at all, if one considers that dynamic stiffness is 10% higher on average than static stiffness according to ratio r, the net increase would fall within the experimentally undetectable variation of 5% (15% becomes 5% when considering average $r = 1.1$; 5% is similar to the 4% of the undetected variation of the pristine condition as described earlier in this section).

Conclusions

A full-scale, three-story, flat-plate concrete building was used to detect damage based on small-amplitude stiffness measurements. Stiffness measured at a maximum 0.03% drift ratio was sensitive to past-large displacements bounded by 3.0% overall drift ratio. Consistency between stiffness measured in static and dynamic tests proved that an elastic nonlinear softening model is a better representation of the actual behavior of the building than the traditional linear model. This study shows that comparing small-amplitude stiffnesses before and after a large-displacement event may be used to detect damage, as long as identical displacements are used (peak displacement if dynamic tests are used). Otherwise, erroneous conclusions may be derived. Given the relationship between damage and small-amplitude stiffness and given the direct connection between stiffness and frequency, use of a nonlinear-elastic dynamic system is recommended: (1) to represent small-amplitude displacement response of; and (2) to detect damage in reinforced concrete structures. As a promising implementation of nonlinear modeling in detection of damage, this research provides a clear example of small-amplitude nonlinear behavior being sensitive to damage in simple terms of stiffness observations in a full-scale building.

As for the proposed model, there are two assumptions and limitations: (1) nonlinearity is assumed to come from stiffness only based on the observation of the pseudo-static load-deflection curve of the building; and (2) the analytical expression $k_o\Delta^{-\alpha}$ used to define the nonlinear softening system at small displacements is an expression that has not been derived from a rational, mechanics-based analysis but is based only on direct observation of the experimental results.

Based on everything mentioned earlier, future works may include: (1) investigation of elastic nonlinearity of reinforced concrete structures at small displacements where vartiations in equivalent damping are taken into consideration; (2) modeling of behavior of reinforced concrete at small displacements so that properties such as the load-displacement curve, which is obtained experimentally, may be estimated from numerical analyses; this could improve our understanding of the nonlinear-elastic behavior at small displacements; and (3) to establish quantitative procedures for estimation of stiffness and frequency degradation at small displacements due to damage.

Data Availability Statement

Some or all data, models, or code that support the findings of this study are available from the corresponding author upon reasonable request.

References

ACI (American Concrete Institute). 2002. *Building code requirements from structural concrete and commentary.* ACI 318. Farmington Hills, MI: ACI.

Adams, D. E. 2010. *Health monitoring of structural materials and components, methods with applications*. Chichester, UK: Wiley.

Bendat, J. S., and A. G. Piersol. 1986. *Random data: Analysis and measurement procedures*. New York: Wiley.

Celebi, M. 1996. "Comparison of damping in buildings under low-amplitude and strong motions." *J. Wind Eng. Ind. Aerodyn.* 59 (2–3): 309–323.

Chang, P. C., A. Flatau, and S. C. Liu. 2003. "Review paper: Structural health monitoring of civil infrastructure." *Struct. Health Monit.* 2 (3): 257–267. https://doi.org/10.1177/1475921703036169.

Chopra, A. K. 1995. *Theory and applications to earthquake engineering*. Hoboken, NJ: Prentice-Hall.

Clinton, J. F., S. C. Bradford, T. H. Heaton, and J. Favela. 2006. "The observed wander of the natural frequencies in a structure." *Bull. Seismol. Soc. Am.* 96 (1): 237–257. https://doi.org/10.1785/0120050052.

Clough, R. W., and J. Penzien. 1975. *Dynamics of structures*. New York: McGraw-Hill.

Consuegra, F., and A. Irfanoglu. 2012. "Variation of small amplitude vibration properties with displacement in reinforced concrete structures." *Exp. Mech.* 52 (7): 817–828. https://doi.org/10.1007/s11340-011-9590-0.

Doebling, S. W. 1996. *Damage identification and health monitoring of structural and mechanical systems from changes in their vibration characteristics: A literature review*. Los Alamos, NM: Los Alamos Laboratory.

Doebling, S. W., C. R. Farrar, and M. B. Prime. 1998. "Summary review of vibration-based damage identification methods." *Shock Vib. Digest* 30 (2): 91–105. https://doi.org/10.1177/058310249803000201.

Durrani, A. J., Y. Du, and Y. H. Luo. 1995. "Seismic resistance of non-ductile slab-column connections in existing flat-slab buildings." *ACI Struct. J.* 92 (4): 479–487. https://doi.org/10.14359/997.

Eberhard, M. O., and M. A. Sozen. 1989. *Experiments and analyses to study the seismic response of reinforced concrete frame-wall structures with yielding columns*. Urbana-Champaign, IL: Univ. of Illinois at Urbana-Champaign.

Elgabry, A. A., and A. Ghali. 1987. "Tests on concrete slab-column connections with stud-shear reinforcement subjected to shear-moment transfer." *ACI Struct. J.* 84 (5): 433–442. https://doi.org/10.14359/1656.

Farhey, D. N., M. A. Adin, and D. Z. Yankelevsky. 1993. "RC flat slab-column subassemblages under lateral loading." *J. Struct. Eng.* 119 (6): 1903–1916. https://doi.org/10.1061/(ASCE)0733-9445(1993)119:6(1903).

Farrar C., K. Worden, M. Todd, G. Park, J. Nichols, D. Adams, M. Bement, and K. Farinholt. 2007. *Nonlinear system identification for damage detection*. LA-14353-MS. Los Alamos, NM: Los Alamos National Laboratory.

Feldman, M. 2006. "Time-varying vibration decomposition and analysis based on the Hilbert transform." *J. Sound Vib.* 295 (3–5): 518–530. https://doi.org/10.1016/j.jsv.2005.12.058.

Fick, D. R. 2010. "Cyclic lateral-load test to failure of a full-scale three-story flat-plate reinforced concrete structure." In *Proc., 9th US National and 10th Canadian Conf. on Earthquake Engineering 2010, Including Papers from the 4th Int. Tsunami Symposium*. Toronto: Earthquake Engineering Research Institute.

Fischinger, M., T. Isaković, K. Kolozvari, and J. Wallace. 2019. "Guest editorial: Nonlinear modelling of reinforced concrete structural walls." *Bull. Earthquake Eng.* 17 (Dec): 6359–6368. https://doi.org/10.1007/s10518-019-00715-z.

Flandrin, P., and J. Stöckler. 1999. *Time-frequency/time-scale analysis*. Paris: Academic Press.

Ghali, A., M. Z. Elmasri, and W. Dilger. 1976. "Punching of flat plates under static and dynamic horizontal forces." *J. Am. Concr. Inst.* 73 (10): 566–572. https://doi.org/10.14359/11097.

Hawkins, N. M., D. Mitchell, and M. S. Sheu. 1974. *Cyclic behavior of six reinforced concrete slab-column specimens transferring moment and shear.* Seattle: Univ. of Washington.

Hwang, S. J., and J. P. Moehle. 2000. "Vertical and lateral load tests of nine-panel flat-plate frame." *ACI Struct. J.* 97 (1): 193–203. https://doi.org/10.14359/849.

Ibarra, L., R. Medina, and H. Krawinkler. 2005. “Hysteretic models that incorporate strength and stiffness deterioration.” *Earthquake Eng. Struct. Dyn.* 34 (12): 1489–1511. https://doi.org/10.1002/eqe.495.

Iwan, W. D., and N. C. Gates. 1979. “Effective period and damping of a class of hysteretic structures.” *Earthquake Eng. Struct. Dyn.* 7 (3): 199–211. https://doi.org/10.1002/eqe.4290070302.

Kolozvari, K., C. Arteta, M. Fischinger, S. Gavridou, M. Hube, T. Isakovic, L. Lowes, K. Orakcal, J. Vásquez, and J. Wallace. 2019. “Comparative study of state-of-the-art macroscopic models for planar reinforced concrete walls.” *ACI Struct. J.* 115 (6): 1637–1657. https://doi.org/10.14359/51710835.

Kovacic, I., and M. J. Brennan. 2011. *The Duffin equation, nonlinear oscillators and their behavior.* Hoboken, NJ: Wiley.

Lakshmanan, N., P. Srinivasulu, and V. S. Parameswaran. 1991. “Post cracking stiffness and damping in reinforced concrete beam elements.” *J. Struct. Eng. (Madras)* 17 (4): 105–111.

Luo, Y. H., and A. J. Durrani. 1995. “Equivalent beam model for flat-slab buildings -Part I: Interior connections.” *ACI Struct. J.* 92 (1): 115–124.

Megally, S., and A. Ghali. 2000. “Punching of concrete slabs due to column moment transfer.” *J. Struct. Eng.* 126 (2): 180–189. https://doi.org/10.1061/(ASCE)0733-9445(2000)126:2(180).

Moehle, J. P., and M. A. Sozen. 1978. “Earthquake-simulation tests of a ten-story reinforced concrete frame with a discontinued first-level beam.” *Civil engineering studies. Structural research series No. 451*. Champaign, IL: Univ. of Illinois at Urbana-Champaign.

Morrison, D. G., I. Hirasawa, and M. A. Sozen. 1983. “Lateral-load tests of R/C slab-column connections.” *J. Struct. Eng.* 109 (11): 2698–2714. https://doi.org/10.1061/(ASCE)0733-9445(1983)109:11(2698).

Neild, S. A. 2001. “Using non-linear vibration techniques to detect damage in concrete bridges.” Ph.D. thesis, Dept. of Engineering Science, Univ. of Oxford.

Oppenheim, A. V., R. W. Schafer, and J. R. Buck. 1999. *Discrete-time signal processing*. Upper Saddle River, NJ: Prentice-Hall.

Pan, A., and J. P. Moehle. 1989. “Lateral displacement ductility of reinforced concrete flat plates.” *ACI Struct. J.* 86 (3): 250–258. https://doi.org/10.14359/2889.

Pan, A. D., and J. P. Moehle. 1992. “An Experimental study of slab-column connections.” *ACI Struct. J.* 89 (6): 626–638. https://doi.org/10.14359/4133.

Robertson, I. N., T. Kawai, J. Lee, and B. Enomoto. 2002. “Cyclic testing of slab-column connections with shear reinforcement.” *ACI Struct. J.* 99 (5): 605–613. https://doi.org/10.14359/12300.

Salawu, O. S. 1997. “Detection of structural damage through changes in frequency: A review.” *Eng. Struct.* 19 (9): 718–723. https://doi.org/10.1016/S0141-0296(96)00149-6.

Sohn, H., C. R. Farrar, F. M. Hemez, D. D. Shunk, D. W. Stinemates, and B. R. Nadler. 2003. *A review of structural health monitoring literature: 1996-2001*. Los Alamos, NM: Los Alamos Laboratory.

Sozen, M. A., and C. P. Siess. 1963. “Investigation of multiple-panel reinforced concrete floor slabs.” *Am. Concr. Inst. J.* 60 (8): 999–1028. https://doi.org/10.14359/7888.

Takeda, T., M. A. Sozen, and N. N. Nielsen. 1970. “Reinforced concrete response to simulated earthquakes.” *J. Struct. Div.* 96 (12): 2557–2573. https://doi.org/10.1061/JSDEAG.0002765.

The MathWorks. 2004. *The language of technical computing*. Natick, MA: MathWorks, Inc.

Tura, C., S. Aydin, U. Yazgan, K. Orakcal, A. Ilki, T. Kabeyasawa, and J. Kang. 2023. “Critical issues in nonlinear modeling of reinforced concrete buildings: Code-compliant modeling approaches and the 2015 E-defense shake table tests on a full-scale 10-story building.” *Bull. Earthquake Eng.* 1–36. https://doi.org/10.1007/s10518-023-01772-1.

Yu, E. 2005. “Forced vibration testing and analytical modeling of a four-story reinforced concrete frame building.” Ph.D. thesis, Dept. of Civil Engineering, Univ. of California, Los Angeles.